J Mater Sci (2007) 42:1838–1846
DOI 10.1007/s10853-006-0956-0

Structural and sensing properties of a novel Fe/Fe_2O_3/polyoxocarbosilane core shell nanocomposite powder prepared by laser pyrolysis

A. Tomescu · R. Alexandrescu · I. Morjan · F. Dumitrache · L. Gavrila-Florescu · R. Birjega · I. Soare · G. Prodan · Z. Bastl · A. Galikova · J. Pola

Received: 15 May 2006 / Accepted: 6 September 2006 / Published online: 14 December 2006

Abstract This paper reports about the synthesis and characterization of a novel Fe/Fe_2O_3/polyoxocarbosilane core shell nanocomposite as a material for gas-sensing applications. The nanocomposites (Fe-based nano cores enveloped with polymeric polyoxocarbosilane shells) were prepared by the IR laser co-pyrolysis of iron pentacarbonyl and hexamethyldisiloxane. The iron-based cores become superficially oxidized in atmosphere. The morphologies, chemical content and thermal behavior were studied by different analytical techniques. The sensing properties of the polymer-poor nanocomposite thick films were tested by measuring the variation of the electrical resistance in presence of CO and CH_4, at a working temperature of 450 °C. Preliminary results indicate that for CO toxic gas, an n–p transitional character of the semiconducting iron oxide appears in humid relatively to dry air.

A. Tomescu
National Institute of Materials Physics, P.O. Box MG-7, RO-077125 Bucharest, Romania

R. Alexandrescu (✉) · I. Morjan · F. Dumitrache · L. Gavrila-Florescu · R. Birjega · I. Soare
National Institute for Lasers, Plasma and Radiation Physics Bucharest, P.O. Box MG-36, R-76900 Bucharest, Romania
e-mail: ralexa@b.astral.ro

G. Prodan
Ovidius University, P.O. Box 8600, Constanta, Romania

Z. Bastl
J. Heyrovsky Institute of Physical Chemistry, Academy of Sciences of the Czech Republic, 182 23 Prague, Czech Republic

A. Galikova · J. Pola
Institute for Chemical Process Fundamentals of the Czech Academy of Science, 165 02 Prague 6, Czech Republic

Introduction

Fundamentally new and often superior physical properties emerge in hybrid materials at the nanoscale. Nanocomposite metal/metal oxide nanoparticles, separated by various polymers [1] are presently promising for a new generation of high temperature gas sensors [2].

Solid state gas sensors, based on the adsorbate dependent electrical conductivity of semiconducting metal oxides, are widely used for detection of harmful gases. If we refer to stannic oxide (SnO_2) as the prototypical solid state gas sensor material, acceptor-like or donor-like adsorption of molecules results in charged adsorbates, which induce a band bending of the energy levels in semiconductors [3]. The resulting variation of charge carriers in the conduction band causes a detectable change in conductivity or 'gas response'.

It is now obvious that nanocrystalline materials, exhibiting small particle sizes and large surface area can be used for gas sensors which require an excellent surface effect. Metal oxide semiconductor (MOS) materials have non-stoichiometric structures, so free electrons originating from oxygen vacancies contribute to the electronic conductivity [4]. Several challenges need to be solved in the development of gas sensors. These include thermal stability, operation at temperatures often greater than 500 °C and both sensitivity

and selectivity (the ability to distinguish between the different gases).

Although a large number of different semiconductor oxides have been investigated for their gas sensing properties, there are few published reports concerning the sensing behavior of pure or doped Fe_2O_3 materials, either as thin films [5], pellets [6, 7] or as thick films [8, 9]. Still fewer reports exist (after our knowledge) in the area of Fe_2O_3 gas sensor optimization by nanoparticle processing, including novel fabrication methods. Many reports underline that the high resistance of a pure iron oxide film limits its practical use as sensor. Addition of dopants decreases the film resistance and induces selectivity in sensor response.

A survey of the literature [10] reveals that polymers also acquired a major position as materials in various sensor devices. Recent reports present either intrinsically conducting polymers, used as coating or encapsulating materials [11] or electrically conductive composites that contain conductive fillers dispersed in an insulating polymer matrix [12]. On the other hand, the incorporation of nanostructured metal oxide with sensing characteristics in polymer matrixes was studied [13, 14] and could be designed to optimize the performances of gas sensors by improving the sensor thermal behavior, the selectivity and the reliability.

We have reported recently on the formation of Fe-based nano cores enveloped with polymeric polyoxocarbosilane shells [15]. The IR laser-induced pyrolysis from gas-phase reactants was used as synthesis technique [16]. A mixture containing iron pentacarbonyl ($Fe(CO)_5$) and hexamethyldisiloxane (HMDSO)—as iron and polymer precursors, respectively and ethylene—as reaction sensitizer was employed [17].

In this paper, the first investigations on gas-sensing properties of the Fe/Fe_2O_3/polyoxocarbosilane nanocomposite are reported. By using different analytical techniques, the chemical structure of the nanocomposite was studied as a function of the $[(CH_3)_3Si]_2O$ content in the gas precursor mixture. The sensing properties of the polymer-poor nanocomposite thick films were tested by measuring the variation of the electrical resistance in presence of CO and CH_4, at a working temperature of 450 °C. Preliminary results indicate the n–p transitional character of the semiconducting Fe_2O_3 toward CO toxic gas in humid relatively to dry air.

Experimental

Materials

The black nanosized composites possessing iron-based cores embedded in polyoxocarbosilane layers were produced in a flow reactor, by the IR laser irradiation of gaseous iron pentacarbonyl and hexamethyldisiloxane, as described in details elsewhere [15]. The focused continuous-wave CO_2 laser radiation (100 W maximum output power, $\lambda = 10.6$ μm) orthogonally crossed the gas flows emerging through three concentric nozzles. $Fe(CO)_5$ vapors (about 25 Torr vapor pressure at 20 °C) entrained by C_2H_4 were admitted through the central inner tube, while HMDSO vapors entered in the reaction cell through an intermediate, middle tube. The carrier gas for HMDSO was either C_2H_4 or Ar. The reactive gas flow was confined to the flow axis by a coaxial Ar stream (the third, outer tube). In order to prevent the NaCl windows from being coated with powder they were continuously flushed with Ar. Since both $Fe(CO)_5$ and HMDSO do not absorb in the 10.6 μm region, C_2H_4 was used as sensitizer (it is excited by the absorption of the CO_2 laser radiation and transfers, by collision the absorbed energy towards the other reaction partners thus finally increasing the translation temperature of the whole system). During the experiment, the pressure in the reactor was maintained constant (450 mbar).

The parameters for two representative runs are presented in Table 1 (the first 4 columns). As opposed to Run PF8 in Table 1, Run PF12 represents samples with lower polymer content. A complementary ethylene flow was necessary in this case for the reaction onset.

The sensitive structures were obtained under the form of thick films by mixing the obtained Fe/polymer nanocomposite with an organic solvent and by depositing them on an alumina support equipped with Pt electrodes and heater. For performing sensing tests, the thick films were calcined at 500 °C (during10 min) thus removing the organic solvent and improving the adherence onto the substrate. The last row of Table 1 refers to the properties of the calcined PF12 sample (heated in air at 500 °C).

Analytical methods used for the characterization of the materials

After synthesis, the morphology and composition of the Fe/polymer nanocomposites were characterized by transmission electron microscopy (TEM), selected area electron diffraction (SAED), X-ray diffraction (XRD), thermal analysis (TGA and DTA) and Infrared Spectroscopy and X-ray photoelectron spectroscopy (XPS).

The XRD pattern was recorded on a DRON DART UM-2 diffractometer equipped with a Cu K_α radiation and a graphite monochromator in the diffracted beam. The crystallite sizes were calculated from the corrected

Table 1 Experimental parameters and XRD estimations of mean crystallite sizes (D) for two significant samples obtained by the laser synthesis of iron-based /polyoxocarbosilane nanocomposites and for the sample heated at 500 °C

Sample	Ethylene/sccm ($Fe(CO)_5$ carrier)	Ethylene/sccm (HMDSO carrier)	Ar/sccm (HMDSO carrier)	Ethylene/sccm (sensitizer)	D(nm) XRD analysis		
					α-Fe	γ-Fe_2O_3/Fe_3O_4	α-Fe_2O_3
PF 8	60	30	–	–	9.5	8.6	–
PF 12	60	–	10	120	9.4	3.4	–
PF12 500 °C	–	–	–	–	–	–	53.5

In both runs the pressure and the laser power were maintained at 450 mbar and 70 Watt, respectively

FWHM (full width and half maximum) applying the Debye–Scherrer formula. The powdery deposits were imaged in a transmission electron microscope Philips CM120ST (Customized Microscope 120 Super Twin, 120 kV max. acceleration voltage, about 2 A resolution, Cs = ~1.2 mm). The samples were analyzed by the different electron microscopy techniques such as BF-TEM (Bright Field Transmission Electron Microscopy), SAED and HRTEM (High Resolution Transmission Electron Microscopy). Thermal analysis of the Fe/polyoxocarbosilane nanocomposites (12–20 mg sample weight) was carried out by heating the samples up to 750 °C at the rate of 4 °C per minute using Cahn D-200 recording microbalances in a stream of argon (flow rate 100 ml/min). X-ray photoelectron spectra were measured with a Gammadata Scienta ESCA 310 electron spectrometer using monochromatized Al Kα ($h\nu$ = 1486.6 eV) radiation for electron excitation. The energy scale of the spectrometer was calibrated with Au $4f_{7/2}$ binding energy fixed at 84.0 eV.

The nanocomposites were tested for the sensing capabilities using a DC—resistance measurement unit equipped with and electronically driven computer controlled Gas Mixing Station [18]. The conductivity measurement facility allows for the determination of the electrical resistance $R = 1/G$ as a function of the temperature (the different temperatures of the active layers), the relative humidity (0–70% humidity) and the gas concentration. The resistance of the films has been monitored during the controlled exposure to 0–500 ppm and 0–5,000 ppm danger levels, in case of CO toxic gas and CH_4 explosive gas, respectively. Different gas atmospheres were obtained by mixing synthetic air (5.0 purity) with methane and carbon monoxide (5.0 purity). During measurements, the temperature of the active layer was maintained at 450 °C and was obtained by applying a constant 8 V voltage to the Pt heater.

However, it was observed that probably due to their high polymer content, most PF samples (including sample PF8) exhibited a higher electrical resistance than the sensor measuring device domain (100 MΩ upper values). It is worth noting that the nanocomposite sample with lower polymer content (sample PF12) which is thoroughly investigated along this report was specifically designed to suit the electrical measurements of the sensitivity.

Results and discussions

Iron-based particles embedded in polymer layers

Studies of $Fe(CO)_5$ sequential decarbonylation by laser pyrolysis [19] revealed the fast removal of carbonyl ligands (first bond energy of 41.5 kcal mol^{-1}), with the formation of metallic iron and CO. The CO_2 laser decomposition of hexamethyldisiloxane occurs via (i) primary cleavage of the Si–C and C–H bonds and (ii) subsequent splits of the Si–O bonds in intermediary products [15].

Based on the experimental facts developed in this work, we suppose that the nucleation in the gas phase of these iron atoms is an essential step for the growth of polymer covered iron nanoparticles. The hot surface of the iron nanoparticles could exert a catalytic activity, speeding up the siloxane monomer decomposition. The thermally released monomer fragments (CH_x, C–OH, –C = O etc) may aggregate and adsorb onto the iron core surfaces, covering them with polyoxocarbosilane sheets. These nanocomposites become partially oxidized in the outer layers upon contact with air and change into Fe/Fe_2O_3 (core) nanobodies surrounded with polyoxocarbosilane layers. Such behavior is indicative of the incomplete coverage by the polymeric matrix or of a porous polymer structure.

TEM analysis

Medium resolution images of the nanoparticles are presented in Fig. 1 for samples PF8 (a) and PF12 (b), respectively. Different morphologies seem to characterize these two samples. Thus, the TEM image for the sample with the higher polymer content reveals nearly spherical balls with a core-shell structure and with cca

10–60 nm sizes. Dark cores encased in a lighter material, presumably of polymeric nature appear. The sample with much lower polymer content (PF12) shows irregular features of the polymer matrix. The particles in the polymer cages seem to coexist with rather elongated dark cores.

An overview TEM image of sample PF12 heated at 500 °C indicates structural changes relatively to the as-prepared sample (Fig. 1c). Irregular particles are observed. Many of them still present a core shell structure but in this case the darkish outer shell seems much thinner and more compact than in the as-prepared structures: it seems that the ''fluffy'', polymer-like character was lost.

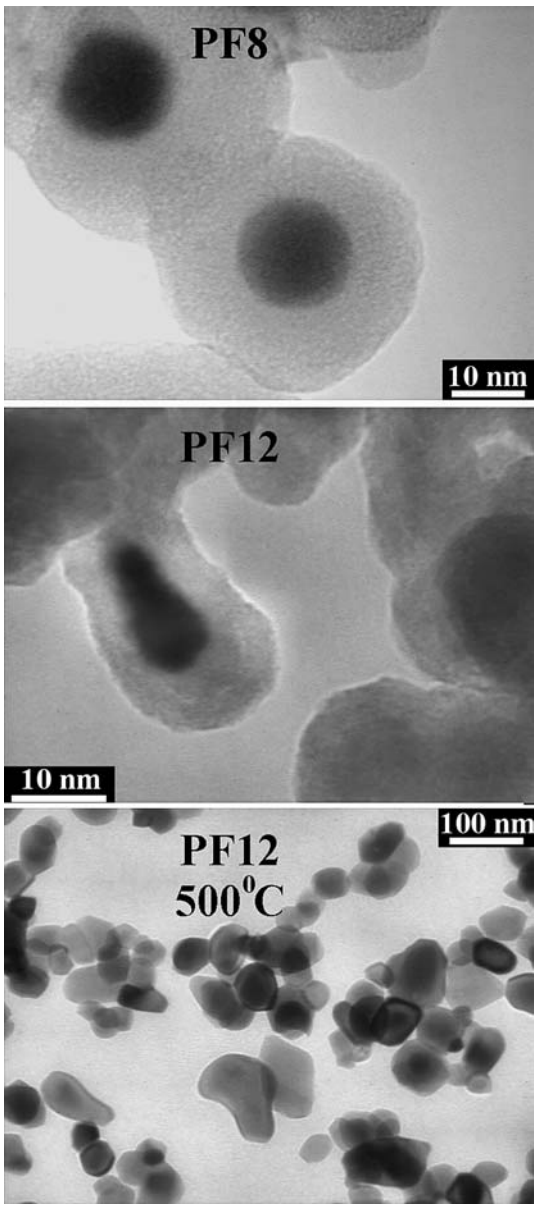

Fig. 1 Medium resolution TEM images of the nanocomposites: (**a**) from Run PF8 and (**b**) from Run PF12; (**c**) low-resolution TEM images of the sample PF12 heated in air at 500 °C

The sharp particle distribution of sample PF12, pointing to a 16.2 nm mean diameter value (maximum value of the Log Normal fitting function) is presented in Fig. 2a. The selected area electron diffraction (SAED) pattern of this sample (Fig. 2b), obtained from a large area of particles exhibits rather diffuse rings (suggesting the formation of amorphous-like or disordered structures) and points to a major presence of γ-Fe_2O_3/Fe_3O_4 (diffraction rings at 2.95, 2.52, 1.61 Å). The presence of the body-centered-cubic bcc α-Fe crystallites (identified by the diffraction ring at 1.17 Å) seems obvious.

The diameter distribution of the heated PF12 sample (Fig. 2c) is still sharp, pointing a mean value of 45.8 nm. This observation is of high importance for the sensing behavior, since it demonstrates the nanometric character of the thick film structure.

XRD analysis

The diffractograms of PF8 and PF12 Fe/polymer nanocomposites exhibit an evident broadness denoting the occurrence of very small particles and/or the presence of an amorphous phase (Fig. 3). In agreement with the SAED analysis, the XRD spectra show the coexistence of two major phases: an oxide phase and an α-Fe phase. The crystalline phase composition and the crystallite dimensions are estimated in the last column of Table 1. In Fig. 3, the angular positions of the broadest peaks are consistent with a spinel-type iron oxide (Fe_xO_y), identified as either magnetite-Fe_3O_4 (JCPDS 19–0629, a = 8.396 Å) or maghemite-γ-Fe_2O_3 (JCPDS 39–1346, a = 8.3515 Å). The peak broadening prevents from undoubtedly distinguish between these two structures. However, the values of the a lattice parameter (8.373 Å and 8.363 Å for PF8 and PF12, respectively) suggest the most likely formation of a maghemite phase. The main difference is related to the Debye–Scherrer crystallites sizes, namely 3.4 nm for PF 12 and 8.6 nm (substantially higher) for PF8. The α-Fe phase (JCPDS file 06-0696) displays similar characteristics in both samples: the same cell parameter a = 2.867 Å equal to the standard 2.8664 Å value and almost equal Debye–Scherrer sizes (see Table 1). The coexistence of γ-Fe_2O_3/Fe_3O_4 and α-Fe was reported by other authors as a result of the oxidation by air exposure [20]. On the other hand, it was found that the exposure of iron to low pressures of dry oxygen gas at room temperature results in an oxide that has been reported to consist qualitatively of a layer of Fe_3O_4 covered by a second layer of γ-Fe_2O_3 [21]. As

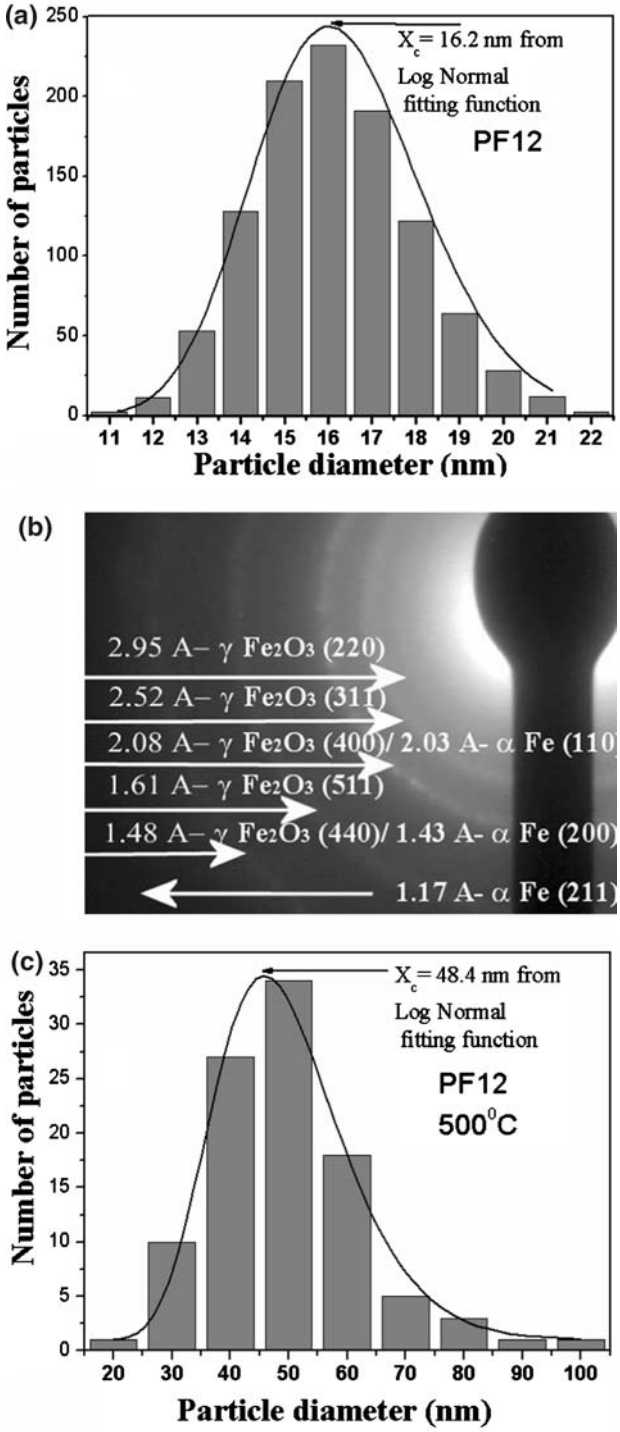

Fig. 2 Particle diameter distribution for sample PF12 (**a**) and for sample PF12 heated in air at 500 °C (**c**); the SAED analysis for sample PF12 (**b**)

mentioned before, the partial oxidation of the nanocomposites occurs in outer layers, upon contact with air and is most probably due to defects in the polymeric shell. A relative larger content of oxides for sample

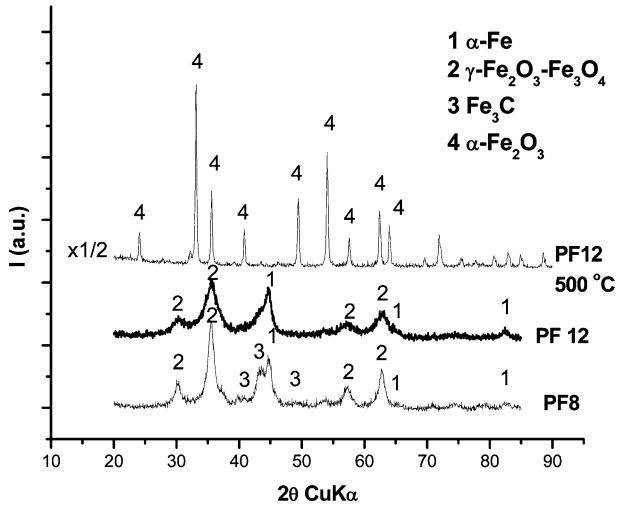

Fig. 3 XRD analysis for samples PF 8 and PF 12, with the identification of the main peaks. The upper curve represents the diffractogram of PF12 sample heated at 500 °C in air, revealing the almost total transformation of the iron-based core in hematite

PF12 is probably related to both a large number of very small Fe particles and the existence of defects in the polymeric coat.

The XRD spectrum of the heated in air PF12 sample (the upper diffractogram in Fig. 3) shows almost entirely the hematite iron oxide phase (JCPDS 33-0664). The estimated mean crystallite size of about 54 nm indicates an expected thermal grain growth. However, the nanosized character of the material is still maintained.

Thermal analysis

The thermal behavior of the powders PF8 and PF12 was examined up to 700 °C. Both powders are rather stable and lose about 12% and 5% of their weight, respectively. The polymer degradation at high temperature in sample PF12 should be rather small since this sample is already characterized by low polymer content. If the weight decrease at around 100 °C is likely due to desorption of traces of water, recent studies [17] have demonstrated that the Fe/Fe_2O_3/polioxocarosilane nanocomposite is subject to depletion by a the Fe/Fe_2O_3 core heterogeneous catalysis. The results of the thermogravimetric analysis/differential thermal analysis (TGA/DTA) of sample PF12 are presented in Fig. 4. The plot shows that that the Fe/Fe_2O_3/polyoxocarbosilane nanocomposite decomposes through a two-stage (at low- and at high-temperatures) evolution of methane. It is shown that in the temperature range 100–700 °C relatively stable C=C and unstable Si=C

bonds are formed. These unsaturated bonds are reactive towards oxygen and water. Consequently, when exposed to air, oxygen bonds (like in Si–O and C=O) are formed.

The IR transmission spectra (not presented here) confirm the findings of the thermal analysis. Referring to the DTA plot, we assume that the broad peak appearing around 500 °C may be related also to phase transformations occurring in the Fe-based content of the nanocomposite. It was shown [8] that for pure (-Fe_2O_3, an exothermic peak appears at about 495 °C which means that a phase transition from spinel structure to corundum structure (α-Fe_2O_3) (irreversible transition) occurs at this point. As concerning the chemical content of sample PF12 heated in air, the main information was derived from XRD analysis, i.e. the major hematite presence. Since after our knowledge there are no reports about the pyrolysis of the polyoxocarbosilanes in air one can speculate about the possible formation of Si–O-based compounds, as indicated by the IR spectra (the low-intensity band around 1,134 cm^{-1}). The formation of SiC was found to occur at higher temperatures (exceeding 1,100–1,200 °C) while at 500–600 °C, free carbon and silica seem to prevail [22].

XPS analysis

The X-ray photoelectron spectra of the superficial layers of the as-prepared and residue (after TGA) nanocomposites offer complementary information about their chemical structure. A detailed discussion about the specific chemical states in polyoxocarbosilane-based composites, in connection with the Si(2p), C(1s) and O(1s) spectra is found in [17]. Here we mention some relevant aspects of the chemical structure which could further contribute to the understanding of the sensing properties. The Fe(2p) spectra reveal the presence of two chemical states of iron, i.e. that of Fe^0 (707.5 eV) and Fe^{3+} (Fe_2O_3, 711.5 eV) [25]. In Fig. 5a, the comparison between the Fe(2p) spectra of PF8 and PF12 samples may be followed. It is shown that the outer layers of the polymer-poor sample contain only the oxidized Fe^{3+} form. Figure 5b presents a comparison between the sample PF12 as prepared and the residue (after thermal analysis). The C(1s) spectra can be decomposed into components at 284.8, 286.7 and 289.2 eV which are assignable to CH_x, C–O and O=C–O moieties [23]. The C1s spectral line of the PF12 residue suggests a depletion in the total C content mainly due to the decrease of C–O and –C=O components.

One should underline the relevance of the structural data for the comparison between the morphologies and chemical content of PF8 and PF12. If the polymer shell is thicker (sample PF8) then, on one hand the dielectric character is higher and on the other hand, the oxidative process of the Fe-based core is lowered, with a deleterious effect on the semiconducting iron oxide formation.

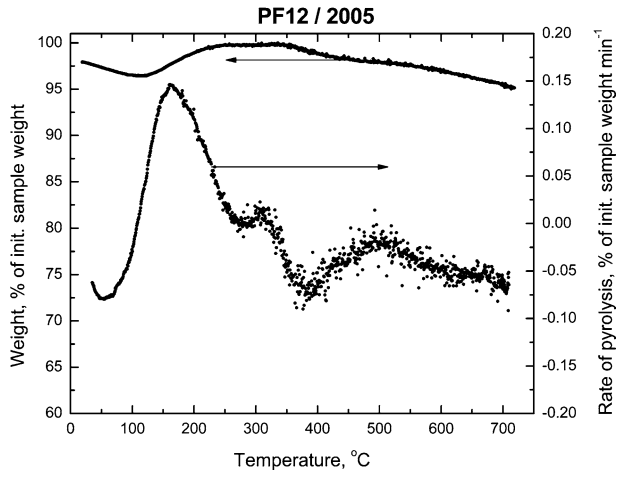

Fig. 4 Thermogravimetric analysis/differential thermal analysis of sample PF12

Sensing behavior of the Fe/Fe_2O_3/polyoxocarbosilane nanocomposite

Gas sensitivity measurements

Assuming a semiconducting gas sensor behavior of the nanocomposite, the cross sensitivity of Fe_2O_3/polyoxocarbosilane thick films was studied by exposing them to carbon monoxide, methane and different humidity levels at a constant temperature of 450 °C. One should observe that for ''in field'' applications, the relative humidity of air cannot be neglected. We consider the selectivity of the system with regard to both these gases since CO is a product of incomplete combustion of CH_4. Figure 6a shows the transient characteristic of the electrical resistance for the PF12 thick film at different concentrations of CH_4 and CO (graphically marked with different types of hachure) in synthetic dry air (left side of the image) and in controlled humidity (right side of the image). The thin solid lines give the schedule of switching and applied gas concentration. The height of the steps corresponds to the concentrations of carbon monoxide (500 ppm) and methane (2,500 ppm), respectively. In dry air atmosphere (0% RH), in the presence of both CO and CH_4 gases the PF12 resistance variation has an increasing trend which points a type p conduction. On the contrary, in humid

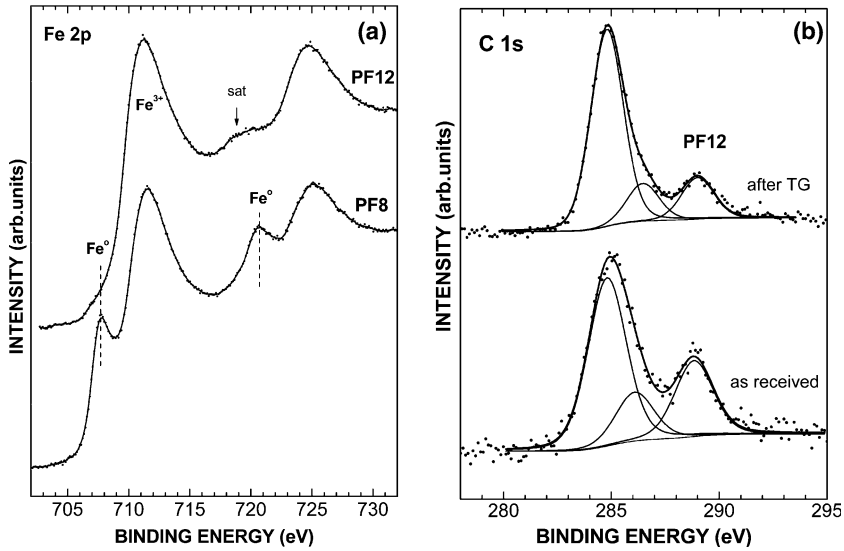

Fig. 5 (**a**) Fe 2p X-ray photoelectron spectra of the powders from Run PF12 and PF8; (**b**) C1s window for PF12, original sample (lower curve) and residue after TG (upper curve)

air atmosphere (30% RH), which is similar to usual practical situations, the variation of PF 12 resistance in presence of CH_4 has a very low increase (type p conduction) but in presence of CO it experiences a decreasing trend (type n conduction). Thus, Fig. 6a reveals the p- to n-transitional character for CO gas in humid relatively to dry air. At the same time, one observes that an incipient selectivity might exist in humid air for the detection of CO (type n conduction) relatively to CH_4 (type p conduction). In order to evaluate the extent of this observed selectivity [24], one needs to increase the sensor response to CO and CH_4 by improving the different technological steps involved in the thick film formation. The nonlinearities in the sensor response (appearing in dry air under the form of spikes) may be due to the unstable reaction centers further inhibited in the presence of water.

Figure 6b displays the temporal variation of the composite resistance for different RH (%). In presence of water the semiconductor conductivity demonstrate a constant p-type behavior. Much more, remarkable stable and reproducible sensor response may be noticed.

Figure 6c displays the plot of the sensor's signal toward both CO and relative humidity (RH %), for different applied gas concentrations and percent RH, respectively. The signal S is defined as the ratio between the resistance of the sensitive film measured in air versus the resistance in the test gas ($S = R_{air}/R_{test}$). Thus, the sensor signal reaches the value of 1.07 for CO concentration of 500 ppm at an operating temperature of 450 °C. Although difficult to compare (due to the different experimental conditions, including the preparation method) this modest value seems however to be higher than that reported by Lee et al. [8] for thick films of iron oxide. At the same time, for the inverse of the sensor signal (defined as $1/S = R_{test}/R_{air}$), a value of 1.35 is reached for 30% relative humidity.

The dependences in Fig. 6c which refer to the sensitivity measurements in CO and humid air are relevant for the n–p transitional character of the semiconducting iron oxide. An n- to p-type conductivity transition induced by oxygen adsorption on α-Fe2O3 was already reported [25]. It was suggested that n- or p-type conduction is observed due to the low formation enthalpy of intrinsic defects, such as oxygen vacancies [26].

We should mention that at this stage, the goal of our preliminary investigations was merely phenomenological, intending to study the cross sensitivity of the sensing structures. An analysis of other sensor parameters, most important for practical applications (such as the response and the recovery time, the sensor calibration curve and its temporal stability, etc) will be the concern of further investigations.

Fe–C nanocomposite as a mixed sensor system

As described before, the Fe/Fe_2O_3/polyoxocarbosilane nanocomposites possess a dominant core-shell structure which could manifest a sensing behavior primary due to the iron—oxide-based core. In this connection, the better material stability offered by the hematite relatively to other iron oxide phases such as maghemite was considered. A nanometric structure, presenting a high surface area will enhance the sensing properties. Indeed, the processing of the sensing material ensures a grain size in the nanometric range, even after air calcination at 500 °C (see Fig. 2). Therefore, the

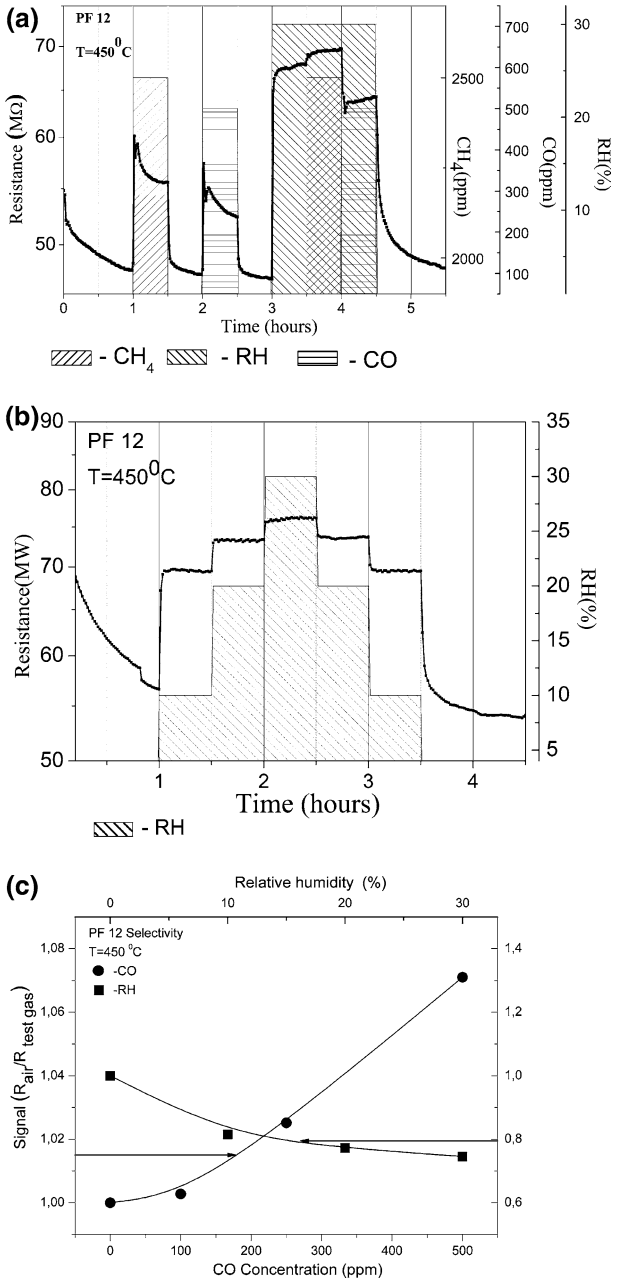

Fig. 6 (**a**) Transient response of the iron oxide/polymer thick film to various CH_4 and CO concentrations in synthetic dry air (left side of the image) and in controlled humidity (right side of the image); (**b**) Transient behavior of the measured electrical resistance for different percent relative humidity values; (**c**) The signal (R_{air}/R_{test}) versus CO concentration and percent relative humidity, respectively, measured at 450 °C working temperature

specific surface exposed to gas reactions should be high enough for sensing applications.

However, for explaining the observed sensitivity one should take into account not only the Fe_2O_3 content but also the polymeric shell. Experimental facts [17] indicate that interactions between the oxide core and the polymer are taking place and that the calcined polyoxocarbosilane shell could play a complex role as far as the sensing properties are concerned: (i) the polymer coating maintain a good dispersion between the small grains (coatings prevents grain growth and agglomeration) thus avoiding sintering and at the same time, probably exceeding the percolation threshold [27]; (ii) if we refer to the polycarbosilanes pyrolysis in the range 100–500 °C, the polymer degradation is low and the polymer shell could act like a stabilizer for the oxide phase at higher temperatures [28]; (iii) however, even in this range of temperatures the thermal degradation begins and should be manifested by the loss of volatile components, by moderate cross-linking and by the formation of an inorganic, ceramic precursor composition (such as carbon-rich, amorphous Si compounds) [29]. Simultaneously, the appearance of nanometric-size channels, due to the loss of gas and shrinkage in volume could favor gas penetration onto the Fe_2O_3 interface [30]; (iv) the probably low contribution of the carbonaceous component of the calcined composite to the semiconductivity of the thick film should not be neglected. In fact it is already known that, depending on the chemical process and on the heating temperature, amorphous carbon (issued from the degraded organic compounds/polymers) could present different degrees of semiconductivity [31].

In addition, the sensing behavior of our system seems to be tightly connected to the different humidity conditions. In this connection, an incipient mechanism may be qualitatively invoked. It was already observed that in case of Fe_2O_3—based thin films, the relative humidity has a strong effect of on the CO response [5]: in dry air, the sensor response is related to the surface reactions between CO and the chemisorbed oxygen but the co-adsorbed water may change states and reactivities of the adsorbed oxygen and consequently, the sensor response.

Conclusions

Initial results concerning the structure and the sensitive behavior of a Fe/Fe_2O_3/polyoxocarbosilane nanocomposite are reported. Nanocomposite powders with different polymer content were prepared by the IR laser co-pyrolysis of iron pentacarbonyl and hexamethyldisiloxane. They become superficially oxidized in atmosphere. Their morphologies, chemical content and thermal behavior were studied by different analytical techniques. Thick films prepared from the low-polymer content Fe-based/polymer material were examined for the sensing capabilities, by testing the variation of the electrical resistance in presence of CO and CH_4 gases.

Preliminary measurements were performed at a temperature of 450 °C, in dry and humid air. It resulted that, relatively to CO toxic gas, an n–p transitional character of the semiconducting iron oxide appears in humid—dry air, respectively. The more stable sensor behavior of the nanocomposite in the presence of different humidity conditions suggests possible applications in the area of humidity sensors. Further studies will focus on the different factors (granulation, crystallinity, doping and calcination temperature) which could improve sensor response and selectivity towards the monitored gases.

Acknowledgements Support of this research by the Project No **4589-CEEX/2006 of the Romanian Ministry of Education and Research**, is gratefully acknowledged.

References

1. Chen W, Yang J, Yang CZ (1997) J Mater Sci 32:3571
2. Han JS, Bredow T, Davey DE, Yu AB, Mulcahy DE (2001) Sens Actuators B 75:18
3. Batzill M, Diebold U (2006) J Phys Condens Matter 18:L129
4. Yang T-Y, Lin H-M, Wei B-Y, Wu CH-Y, Lin CH-K (2003) Rev Adv Mater Sci 4:48
5. Neri G, Bonavita A, Galvagno S, Siciliano P, Capone S (2002) Sens Actuators B 82:40
6. Han JS, Bredow T, Davev DE, Yu AB, Mulcahv DE (2001) Sens Actuators B 75:18
7. Tianshu Z, Hongmei L, Huanxing Z, Ruifang Z, Yusheng S (1996) Sens Actuators B 32:181
8. Lee D-D, Choi D-H (1990) Sens Actuators B I:231
9. Malyshev VV, Eryshkin AV, Koltypin EA, Varfolomeev AE, Vasiliev AA (1994) Sens Actuators B 18–19:434
10. Adhikari B, Majumdar S (2004) Prog Polym Sci 29:699
11. Haug M, Schierbaum KD, Endres HE, Drost S, Goepel W (1992) Sens Actuators A 32:326
12. Bloor D, Donnelly K, Hands PJ, Laughlin P, Lussey D (2005) J Phys D Appl Phys 38:2851
13. Sawicka KM, Prasad AK, Gouma PI (2005) Sens Lett 3:1
14. Yu J, Liu RYF, Poon B, Nazarenko S, Koloski T, Vargo T, Hiltner A, Baer E (2004) J Appl Polym Sci 92:749
15. Pola J, Marysko M, VorlU+00Alcek V, Bastl Z, Galýkov A, Vacek K, Alexandrescu R, Dumitrache F, Morjan I, Albu L, Prodan G (2005) Appl Organometal Chem 19:1015
16. Alexandrescu R, Morjan I, Dumitrache F, Voicu I, Soare I, Sandu I, Fleaca CT (2004) Solid State Phenom 99–100:181
17. Galíková A, Bastl Z, Alexandrescu R, Morjan I, Pola J (2005) Thermochim Acta 439:80
18. Roescu R, Dumitriu I, Tomescu A (2004) Rom Reports Phys 56:607
19. Dumitrache F, Morjan I, Alexandrescu R, Morjan RE, Voicu I, Sandu I, Soare I, Ploscaru M, Fleaca C, Ciupina V, Prodan G, Rand B, Brydson R, Woodword A (2003) Diam Relat Mater 13:362
20. Bi X-X, Granguly B, Huffman GP, Huggins FE, Endo M, Ecklund P (1993) Can J Mater Res 8:1666
21. Grosvenor AP, Kobe BA, Mcintyre NS (2004) Surf Sci 565:151
22. Choi JY, Moon YT, Kim DK, Kim CH (1998) J Am Ceram Soc 81(9):2294
23. NIST X-ray Photoelectron Spectroscopy Database, ver. 2.0, US Department of Commerce, NIST, Gaithersburg, MD 20899, USA, 1997
24. Brahim-Belhouari S, Bermak A, Shi M, Chan PCH (2005) IEEE Sens J 5:1433
25. Gurlo A, Barsan N, Oprea A, Sahm M, Sahm T, Weimar U (2004) Appl Phys Lett 85:2280
26. Van de Krol R, Tuller HL (2002) Solid State Ionics 150:167
27. Schmelzer J Jr., Brown SA, Wurl A, Hyslop M, Blaikie RJ (2002) Phys Rev Lett 88:226802
28. Pola J, Ouchi A, Vacek K, Galíková A, Blechta V, Bohǎcek J (2003) Solid State Sci 5:1079
29. Interrante LV, Moraes K, Liu Q, Lu N, Puerta A, Sneddon LG (2002) Pure Appl Chem 74 11:2111
30. Varghese OK, Grimes CA (2003) J Nanosci Nanotechnol 3:277
31. Kuroda H, Flood EA (1961) Can J Chem 39:1475